Synchrotron x-ray diffraction and Raman scattering investigations of $(Li_xNa_{1-x})NbO_3$ solid solutions: Evidence of the rhombohedral phase

Yu. I. Yuzyuk,[1,2] E. Gagarina,[2] P. Simon,[1] L. A. Reznitchenko,[2] L. Hennet,[1] and D. Thiaudière[1,3]
[1]*Centre de Recherches sur les Materiaux à Haute Temperature, CNRS UPR 4212, F45071, Orléans, France*
[2]*Institute of Physics, Rostov State University, Stachki 194, Rostov-on-Don, 344090 Russia*
[3]*LURE, Centre Universitaire Paris-Sud, Bâtiment 209D, F91198 Orsay, France*
(Received 9 May 2003; revised manuscript received 28 August 2003; published 6 April 2004)

The $(Li_xNa_{1-x})NbO_3$ perovskite solid solutions are investigated using synchrotron x-ray diffraction and Raman spectroscopy in order to clarify the structural changes in the concentration range $0 \leqslant x \leqslant 0.145$ at room temperature. The orthorhombic antiferroelectric *P* phase (space group *Pbma*, $Z=8$) exists up to $x=0.02$ and in the concentration interval $0.02 \leqslant x \leqslant 0.03$ we have confirmed a previously reported transition to the orthorhombic ferroelectric *Q* phase (space group $P2_1ma$, $Z=4$). It is found that the *Q* phase is stable up to $x=0.145$ but in the narrow concentration interval at $x=0.12$ the dominating (86.2%) rhombohedral N phase (space group $R3c$, $Z=2$) coexists with the minor (13.8%) *Q* phase at room temperature. The crystal structure of this rhombohedral *N* phase has been refined using Rietveld method. Detailed comparison with similar low-temperature phase of pure $NaNbO_3$ showed that the NbO_6 octahedra are slightly distorted in the solid solution with $x=0.12$ while they are rather regular in $NaNbO_3$. Raman spectra showed drastic changes associated with the *P*-*Q* transition and revealed coexistence of the *P* and *Q* phases in the interval $0.02 \leqslant x \leqslant 0.03$. Abrupt transformation of the Raman response and remarkable narrowing of the Nb-O stretching vibrations related to the existence of the rhombohedral *N* phase at $x=0.12$ were observed.

DOI: 10.1103/PhysRevB.69.144105 PACS number(s): 61.10.Nz, 63.20.−e, 77.80.−e, 77.84.Dy

I. INTRODUCTION

The ABO_3 perovskite compounds of interest for technological applications are usually *A*- or *B*- substituted solid solutions with a composition close to the so-called morphotropic phase boundary where very high piezoelectric figures of merit are observed. High-density $(Li_xNa_{1-x})NbO_3$ (LNN) ceramics exhibit high sound velocities (>5.5 km/s), low dielectric permittivity (50–100), and very good room-temperature electromechanical properties attractive for high-frequency (>30 MHz) applications. Although ceramics within the system LNN were a subject of numerous investigations[1–11] since 1958, their complete *T*-*x* phase diagram is not yet well understood. In the Na-rich region LNN solid solutions have perovskite-like structure based on a network of corner-linked NbO_6 octahedra. In the Li-rich region the oxygen octahedra are linked together by common faces along the threefold axis and form ilmenitelike (or pseudoilmenite) structure. Currently available information concerning crystal structure of LNN solid solutions for $x<0.15$ is rather controversial. Krainik[1] has reported that LNN solid solutions exhibit antiferroelectric (AFE) properties up to $x=0.01$, whereas further increasing of Li content induces ferroelectric (FE) state. Nitta[2] has studied LNN solid solutions up to $x=0.14$ and suggested pseudomonoclinic-pseudotetragonal room-temperature phase transition for $x=0.12$ (LNN12). Later, the AFE-FE transition from the nonpolar orthorhombic phase *P* to the polar orthorhombic phase *Q* in LNN solid solutions was reported for $x=0.03$, moreover, a rhombohedral FE phase and anomalies of physical properties were revealed in the narrow concentration interval at around $x=0.125$ and *T*-*x* phase diagram for $0 \leqslant x \leqslant 0.145$ was reported.[3–5] Henson *et al.*[6] have studied dielectric and electromechanical properties of LNN ceramics in the concentration range $0.015 \leqslant x \leqslant 0.15$ and reported quite different *T*-*x* phase diagram. The anomalies of dielectric permittivity and electromechanical coupling coefficient for compositions around $x=0.12$ at room temperature were interpreted as an evidence of the transition between orthorhombic and tetragonal phases. Von der Mühll *et al.*[7] disclosed an intermediate rhombohedral $R3c$ phase in the concentration range $0.14 \leqslant x \leqslant 0.17$ which corresponds to heterophase state previously reported by other authors.[3–6] Recent Raman and x-ray diffraction (XRD) studies[8,9] of LNN ceramics revealed no structural peculiarities in LNN12 at room temperature. Neither morphotropic phase boundary between orthorhombic and tetragonal phases nor rhombohedral phase were found at $x=0.12$. Raman measurements[8] revealed phase transitions from the orthorhombic to the rhombohedral $R3c$ (so-called *N* phase in pure $NaNbO_3$) far below room temperature for all compositions with $x \leqslant 0.15$. Very recent structural reexaminations of LNN system[10,11] confirmed that the prototype perovskite cell is rhombohedrally distorted and doubled for compositions around $x=0.12$ at room temperature. It does not follow that the symmetry is rhombohedral too. It may be hexagonal. No detailed direct structural study of the *N* phase in LNN solid solutions at $x=0.12$ was performed up to now and the exact space group was not determined.

The origin of the remarkably enhanced piezoelectric properties at $x=0.12$ deserves further clarification and precise investigations of the crystal structure. In the present paper we report synchrotron XRD and Raman reexamination of pressure-sintered LNN ceramics. Our results show clearly that the rhombohedral phase exists at room temperature in narrow concentration interval around $x=0.12$.

II. EXPERIMENTAL DETAILS

High-density (99.8%) LNN ceramics were prepared by the solid-state reaction of stoichiometric quantities of Na_2CO_3 (99.8%), Li_2CO_3 (99.7%), and Nb_2O_5 (98.7%). All ceramic samples were synthesized using a two-stage annealing at 850–900 °C for 4–5 h at each stage. The components were mixed in ethanol to avoid hydrolysis and milled in water. Sintering was carried out at 1050–1250 °C and pressure 20–40 MPa for 40 min. Fine granular powders for XRD measurements and chemical analysis were prepared by crushing ceramic specimens. Chemical analysis (Service Central analyze, CNRS, Vernaison, France) revealed no remarkable deviations from the batching values of Li/Na content. Synchrotron XRD measurements were performed on the H10 beamline[12] at LURE/DCI (Orsay, France). A monochromatic radiation ($\lambda = 1.304\,23$ Å) was obtained using a double crystal Si(111) monochromator. Powder diffraction patterns were recorded in the Bragg-Brentano geometry in the angular interval 12°–102 ° with a constant 0.016 ° step and a counting time of 1 s per step. Raman measurements were performed on polished ceramic specimens $0.5\times2\times2$ mm. Raman spectra were excited with the polarized light of an Ar^+ laser ($\lambda = 514.5$ nm) and analyzed using a Jobin Yvon T64000 spectrometer equipped with a charge-coupled device. All spectra were obtained in backscattering geometry using a microprobe device that allows the incident light to be focused on the sample as a spot of about 3 μm in diameter.

III. RESULTS AND DISCUSSION

A. X-ray diffraction

The room-temperature XRD patterns for $x=0$ and $x=0.04$ show the splitting of the main Bragg reflections corresponding to the monoclinically distorted perovskite subcell where $a=c>b$ and $\alpha=\gamma=90°<\beta$ (Fig. 1). The superlattice reflections and the rules of systematic absence indicated the following orthorhombic unit cells and the space groups: $\mathbf{A}=\mathbf{a}-\mathbf{c}$, $\mathbf{B}=4\mathbf{b}$, $\mathbf{C}=\mathbf{a}+\mathbf{c}$, $Pbma-D_{2h}^{11}$ (P phase) for $x=0$ and $\mathbf{A}=\mathbf{a}-\mathbf{c}$, $\mathbf{B}=2\mathbf{b}$, $\mathbf{C}=\mathbf{a}+\mathbf{c}$, $P2_1ma-C_{2v}^2$ (Q phase) for $x=0.04$. These results are well consistent with previous studies of P and Q phases in $NaNbO_3$ (Refs. 13–15) and LNN (Ref. 16). The P-Q transformation is clearly illustrated in Fig. 1 where in the XRD pattern for $x=0.04$ the 211, 230, 112, and 151 superlattice reflections related to the quadruplicate parameter b disappear and the 201 reflection appears. In the orthorhombic P and Q phases the NbO_6 octahedra are tilted in a different manner. Following Glazer's structural description,[17] the phase P has pairs of alternating layers: $a^-b^+a^-$ and $a^-b^-a^-$ while in the Q phase the tilting can be described as $a^-b^+c^-$.

XRD patterns for composition where $x=0.11$ and $x=0.13$ are well consistent with the Q phase, whereas for $x=0.12$ the diffraction pattern clearly shows the abrupt change in the splitting of the main reflections (Fig. 1). Examination of the diffraction data revealed the rhombohedral perovskite cell with the parameters: $a=b=c=3.9019$ Å, $\alpha=\beta=\gamma=89.08°$ (phase N). In the N phase the superlattice

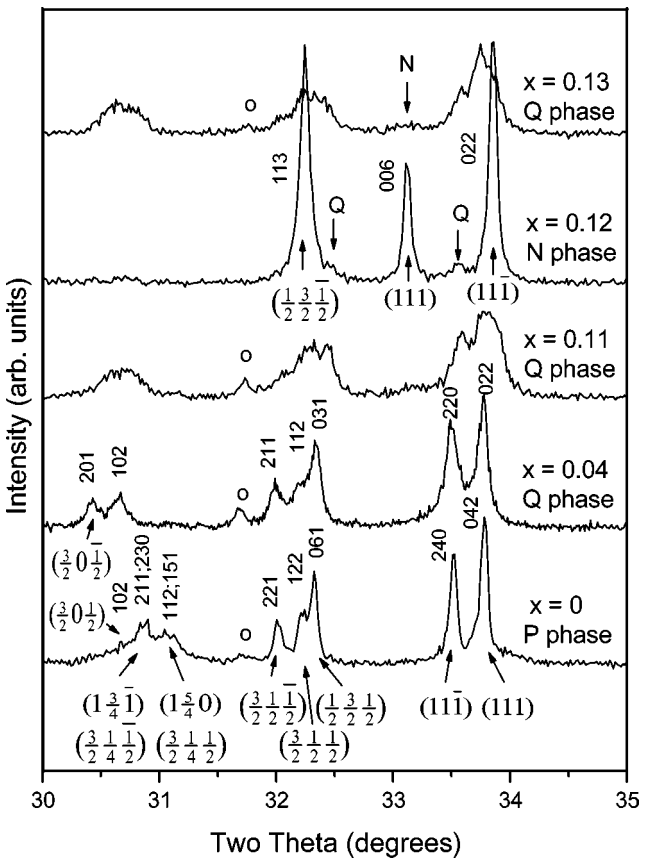

FIG. 1. Portions of the synchrotron diffraction patterns for LNN solid solutions showing the transformations of the superlattice and the main reflections for samples with different Li content. The indices of the reflections referred to the pseudocubic perovskite subcell are given in brackets. Circles and arrows mark the peaks due to the weak impurity of $NaNb_3O_8$ and second phase, respectively.

reflections referred to the perovskite subcell have only half-integer indices such as $(1/2,3/2,-1/2)_p$. This feature implies that the oxygen octahedra are tilted as $a^-a^-a^-$ and suggests the space group $C_{3v}^6=R3c$ (Refs. 17 and 18). For description of the crystal structure we used the following hexagonal axes: $\mathbf{a}_h=\mathbf{b}-\mathbf{c}$, $\mathbf{b}_h=\mathbf{c}-\mathbf{a}$ and $\mathbf{c}_h=2\mathbf{a}+2\mathbf{b}+2\mathbf{c}$. The hexagonal unit cell contains six formula units, while the true unit cell is the primitive rhombohedron ($a_r=5.5622$ Å, $\alpha_r=58.95°$) containing two formula units.

The powder diffraction pattern for $x=0.12$ has been analyzed by Rietveld refinements using FULLPROF (Ref. 19) software. A detailed inspection revealed the presence of the dominant phase N and the minority of the phase Q plus negligible amount of the $NaNb_3O_8$ impurity. The structural parameters for the N and Q phases taken from Refs. 14, 18, and 20 were used as starting point for the refinements. Na and Li atoms were statistically distributed over the same crystallographic site and kept fixed at nominal composition. Slight variations of the Li/Na ratio did not affect the calculated intensities of the XRD peaks. At the first step we determined the unit cell parameters and the profile parameters for both phases using structural dependent and independent fits. The pseudo-Voigt function was chosen to define the peak profiles. It is worth noting that the unit cell volume of the orthorhom-

TABLE I. Final structural parameters for $(Li_xNa_{1-x})NbO_3$ with $x=0.12$ at room temperature.

Phase *N*: Space group $R3c$; $a_h=5.47398(7)$ Å, $c_h=13.7313(1)$ Å; $V_h=356.326(2)$ Å^3; Fract. (%): 86.2(5)					
Atom	x	y	z	B_{eq} (Å^2)	$\beta\times10^4$
Na/Li	0	0	1/4 + 0.0080(14)	1.60(8)	
Nb	0	0	0 + 0.0136(6)	0.377	$\beta_{11}=62(3)$
					$\beta_{33}=0.3(2)$
O	1/6 − 0.0607(9)	1/3 + 0.0163(18)	1/12	1.65	$\beta_{11}=111(20)$
					$\beta_{22}=121(22)$
					$\beta_{33}=27(5)$
					$\beta_{12}=-99(1)$
					$\beta_{13}=-15(1)$
					$\beta_{23}=10(1)$
Phase *Q*: space group $P2_1ma$; $a=5.5662(1)$ Å, $b=7.7467(1)$ Å, $c=5.4949(1)$ Å; $V=236.943(7)$ Å^3; Fract. (%): 13.8(2)					
R factors: $R_p=9.45\%$, $R_{wp}=12.5\%$, $R_{exp}=7.39\%$, $\chi^2=2.84\%$; $R_B=3.94\%$, $R_F=2.59\%$ for the phase *N*; $R_B=4.4\%$, $R_F=3.5\%$ for the phase *Q*					

bic phase *Q* steadily decreases with increasing of Li content. The observed value of the unit cell volume of the minor *Q* phase at $x=0.12$ was found consistent with the nominal Li/Na ratio in this sample. The unit cell volume of the minor phase *Q* in the sample with $x=0.12$ was found smaller than corresponding value for $x=0.11$ but larger with respect to that for $x=0.13$. Therefore, both *Q* and *N* phases contain very close amount of Li atoms and no detectable deviations from the nominal stoichiometry occured. At the second step structural parameters of the *N* phase were refined. Since the structure of the *N* phase is rather simple the anisotropic thermal parameters of Nb and O atoms were tried to refine at the final step and a decreasing of the *R* factors, particularly the R_B one, was achieved. The final structural parameters are given in Table I, where the positions of the atoms are described in terms representing the atomic shifts from the ideal perovskite positions.

The structure of the *N* phase of LNN12 can be described as planar and equidistant oxygen layers (spaced $c_h/6$ apart) perpendicular to the $\mathbf{c}_h$ axis. As one can see in Figs. 2(a, b) these layers are formed by alternation of oxygen octahedra and cubo-octahedra linking together by common faces along the $\mathbf{c}_h$ axis. The Na/Li and the Nb cations are displaced along the polar axis from their positions in the ideal perovskite structure. According to Refs. 18 and 21 the structure of the rhombohedral *N* phase may be derived from the ideal perovskite ABO_3 through the tilting of the BO_6 octahedra around triad axis in opposite directions, as shown in Fig. 2(c). The calculated tilt angle ω using parameters presented in Table I for LNN12 is 12.8°. This value is a little bit larger relative to that in the *N* phase of $NaNbO_3$ at −150 °C (Ref. 18). The structural data reported by Darlington and Megaw[18] for $NaNbO_3$ together with the bond lengths obtained for LNN12 from the present refinement are given in Table II. Note in this connection a decrease of the volume ($V_p=59.68$ Å^3 for $NaNbO_3$ and $V_p=59.39$ Å^3 for LNN12) and an increase of the degree of the distortion ($\alpha=89.21°$ for $NaNbO_3$ and $\alpha=89.08°$ for LNN12) of the perovskite subcell.

Tilting of octahedra leads to difference in the length of *A*-O bonds: there are three long *A*-O3 bonds and three short *A*-O4 ones [Fig. 2(c)]. An enhancement of this difference in LNN12 corresponds to an increase of the tilt angle ω. The length of the *A*-O4 bonds is markedly smaller than in $NaNbO_3$. In contrast to $NaNbO_3$ the oxygen octahedra in LNN12 are distorted due to the O displacement along the $\mathbf{b}_h$ axis from their positions with $y=1/3$. The faces of the octahedra perpendicular to the $\mathbf{c}_h$ axis become not equal: the length of the O2-O2 bonds is longer than that one of the O1-O1 bonds. The Nb atom is displaced to the center of the triangular face with the longer O2-O2 bonds. On the contrary, the Na/Li atom is shifted to the face with the shorter O1-O1 bonds forming stronger bonds with the O4 than with the O1. While the off-center shifts of both Nb and Na/Li decrease in comparison with $NaNbO_3$, the Na/Li shift shows a sharper decrease. Note that the Nb-O2 distance is smaller than the sum of the ionic radii of Nb^{5+} and O^{2-} (2.03 Å), indicating a strong bond.

The Nb environment with anisotropic displacement ellipsoids is shown in Fig. 3. As one can see, the Nb thermal vibrations ellipsoid is a flattened disk perpendicular to the polar axis. The thermal vibrations of O are also strongly anisotropic. The smallest and largest thermal amplitudes for O have been observed roughly along and normal to the directions of Nb-O bonds, respectively (the O1-Nb-O2 bond angle is 168.7°). The form of these ellipsoids corresponds to rotation of the NbO_6 octahedra. This feature along with relatively high thermal parameter values of oxygens points to an instability of the structure with respect to the octahedra tilting about the triad axis.

Further increasing of Li content in LNN solid solutions leads to further distortion of the oxygen framework towards hexagonal-close-packing structure: a decrease of the unit cell volume and an increase of the tilt angle. This particularly concerns the Na environment because the tilts of the octahedra strongly compress Na-O bonds. Apparently, at $x=0.12$ a limiting structure distortion is reached and above this value

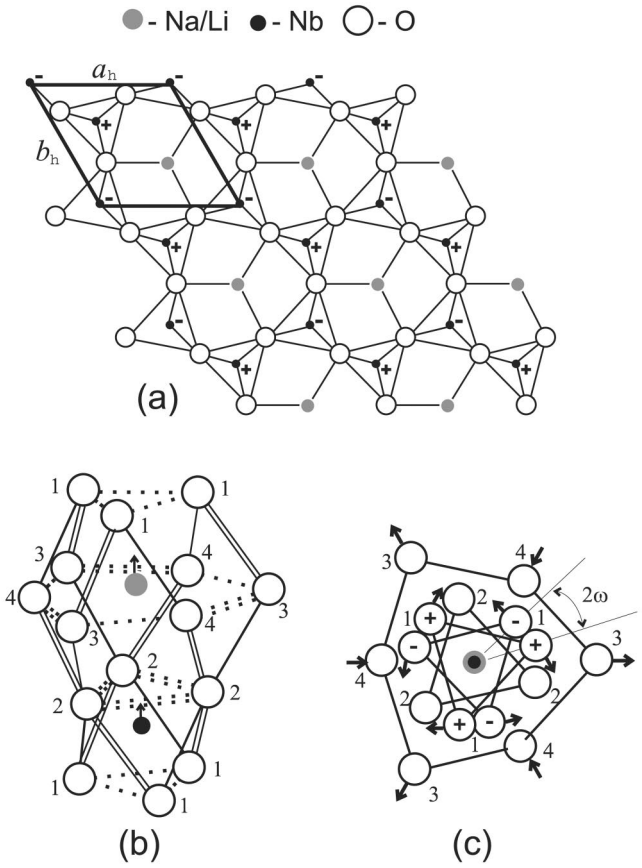

FIG. 2. Schematic views of the $(Li_xNa_{1-x})NbO_3$ structure with $x=0.12$ in the *N* phase. (a) The view of the (001) layer containing the Na/Li and O atoms. The Nb atoms at height 1/12*c* below (−) and above (+) and the base of the hexagonal unit cell are also shown. (b) The alternation of oxygen octahedra and cubo-octahedra along the triad axis. Arrows show the off-center shifts of Nb and Na from the ideal perovskite positions. The different types of the lines correspond to the different lengths of O-O bonds; the doubled lines indicate the longer O3-O4 and O1-O2 bonds. (c) Projection down the triad axis of the structure fragment given in (b). Arrows show the displacements of the O1, O3, and O4 atoms due to the octahedra tilting. Signs (+) and (−) indicate the O1 atoms above and below the O3-O4 plane, respectively.

the Q phase dominates again up to $x=0.145$ that is the upper solubility limit of Li in $NaNbO_3$. The character of thermal motions indicating large rotational instability also points to the possibility of such a change.

B. Raman spectra

The group theory treatment provides a number of Raman-active modes in each phase of LNN solid solutions. Standard factor-group analysis yields the following results:

$$\text{P phase } (Pbma, Z=8)\ \Gamma_{opt} = 15A_g(R)+17B_{1g}(R)+15B_{2g}(R)+13B_{3g}(\text{R}) + 13A_u(-)+14B_{1u}(\text{IR})+16B_{2u}(\text{IR})+14B_{3u}(\text{IR}),$$

TABLE II. Interatomic distances (less then 3.2 Å) in the phase *N* for $(Li_xNa_{1-x})NbO_3$ with $x=0.12$ and $NaNbO_3$.

Atoms	LNN12 (this work)	$NaNbO_3$ (Ref. 18)
Nb-O1	2.043(8)	2.122
Nb-O2	1.951(8)	1.862
Na/Li-O1	2.673(17)	2.560
Na/Li-O2	2.940(17)	3.050
Na/Li-O3	3.117(8)	3.100
Na/Li-O4	2.364(7)	2.423
O1-O1, O3-O4	2.684(11)	2.806
O2-O2, O3-O4	2.944(12)	2.806
O1-O2, O1-O4, O2-O3	2.792(6)	2.803
O1-O2, O1-O3, O2-O4	2.828(7)	2.803

[a]See Fig. 2.

$$\text{Q phase } (P2_1ma, Z=4)\ \Gamma_{opt} = 16A_1(\text{IR},\ R)+13A_2(R)+12B_1(\text{IR},\ R) + 16B_2(\text{IR},\ R),$$

$$N \text{ phase } (R3c, Z=2)\ \Gamma_{opt} = 4A_1(\text{IR},R)+5A_2(-)+9E(\text{IR},\ R),$$

where the IR and *R* activities are denoted in the brackets. In principle, *P*, *Q*, and *N* phases could be distinguished in a polarized Raman study of single-crystalline samples. This discrimination is not straightforward for ceramic samples where all modes appear simultaneously and Raman spectra are unpolarized. Nevertheless, in the rhombohedral *N* phase one can expect a much more simple spectrum with respect to those in *P* and *Q* phases.

Room-temperature Raman spectra of LNN ceramics are presented in Fig. 4. Raman response of $NaNbO_3$ ceramic sample shows very similar overall view and is well consistent with previously reported Raman investigations of ceramics,[8] polycrystalline powders,[23–25] and single crystals.[26] All spectra were carefully fitted with a classical damped multioscillator model. The concentration dependence of the frequencies of all well-defined Raman bands is shown in Fig. 5. Very weak and poorly defined peaks at

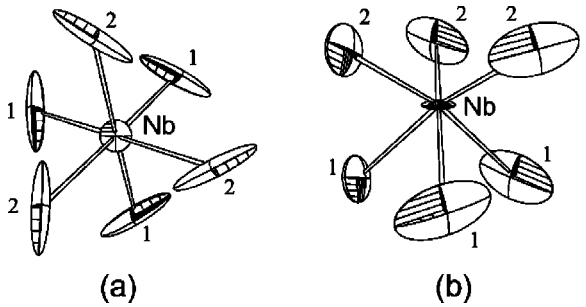

FIG. 3. Projections of the NbO_6 octahedron with anisotropic displacement ellipsoids down (a) and along (b) the triad axis [ORTEP (Ref. 22), 90% probability].

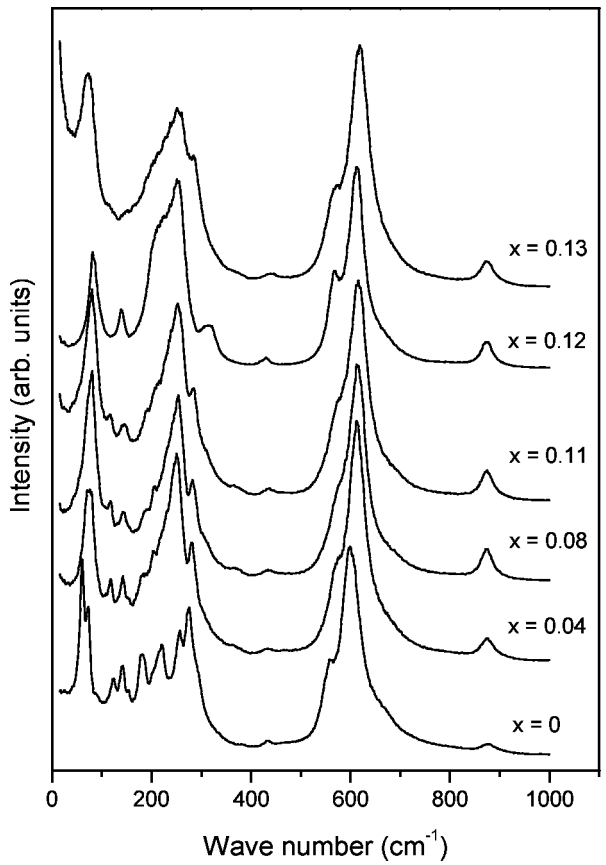

FIG. 4. Raman spectra of $(Li_xNa_{1-x})NbO_3$ solid solutions for selected concentrations.

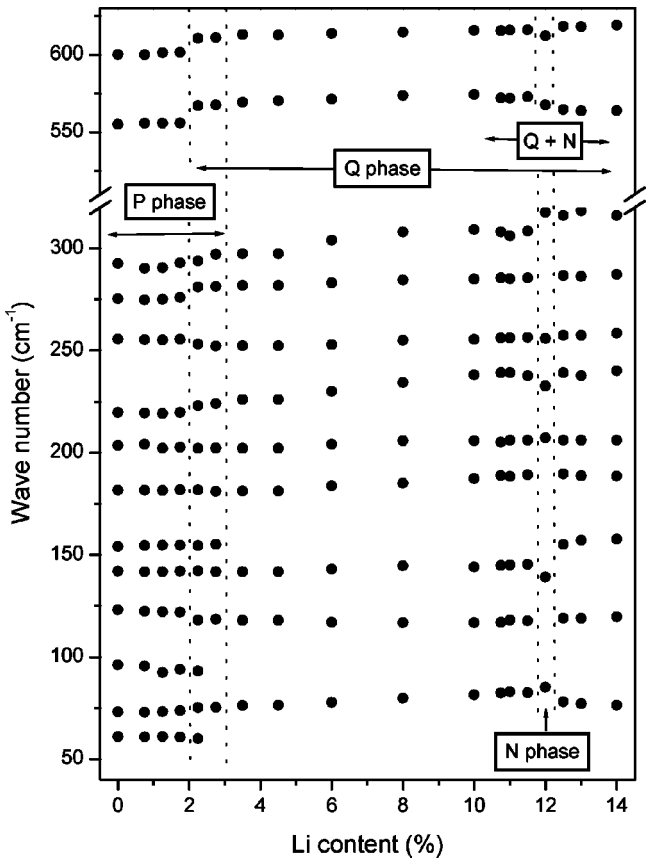

FIG. 5. Frequencies of the Raman peaks in $(Li_xNa_{1-x})NbO_3$ solid solutions as a function of Li content.

around 400 cm^{-1} are not shown. Also, uncertain impurity band at 875 cm^{-1} appears in all ceramic samples. This band was also observed by Juang *et al.*[8,9] and assigned to overtone. This band is independent of the Li content and was excluded in the following discussion. In contrast to Ref. 8 we observed drastic transformations of Raman spectra associated with the structural changes in the concentration range $0 \leqslant x \leqslant 0.14$. The first obvious change occurs in the concentration range $0.02 \leqslant x \leqslant 0.03$: (i) Raman response below 400 cm^{-1} acquires a different spectral fingerprint compared with pure $NaNbO_3$; (ii) two lowest-lying lines at 61 and 73 cm^{-1} merge into a single peak centered at 76 cm^{-1}; (iii) two weak bands at 96 and 154 cm^{-1} lose their intensity and disappear in Raman spectra for $x > 0.03$; (iv) the high-frequency Nb-O stretching bands exhibit upward shift from 557 and 601 cm^{-1} at $x = 0.02$ up to 567 and 610 cm^{-1} at $x = 0.0225$, respectively; (v) the low-frequency component of this doublet shows stepwise broadening at $x = 0.0225$. These effects appear associated with the *P*-*Q* transition. Inspection of our spectra shows that *P* and *Q* phases coexist in the concentration interval $0.02 \leqslant x \leqslant 0.03$.

We attribute the abrupt hardening of the stretching vibrations at *P*-*Q* transition to the displacement of the Nb ions. According to Ref. 15, in the *P* phase, the Nb ion is displaced from the geometrical center of regular octahedron by 0.13 Å in a direction lying almost exactly in the plane of the O(3), O(4) oxygen square and making an angle of 21° with the diagonal of the square. In this environment the Nb-O(4) bond is longer (and therefore weaker) than Nb- O(3) one. In the *Q* phase the Nb displacement is nearly symmetrical and oriented towards the midpoint of the edge. Therefore, in the *Q* phase these two bonds become equal and more likely stronger.

The second significant change occurs at $x = 0.12$. In agreement with the factor group analysis, we have observed a very simple Raman spectrum for this composition. As one can see in Fig. 5, three peaks at 118, 189, and 285 cm^{-1} are missing at $x = 0.12$. Abrupt transformation of the Raman response and its simple overall view well correlate with the rhombohedral symmetry revealed by means of XRD in the above section. In the concentration intervals $0.10 \leqslant x < 0.12$ and $0.12 < x \leqslant 0.14$ Raman spectra suggest coexistence of the minor *N* phase with the major *Q* phase. Enhanced Rayleigh scattering observed in the above-mentioned concentration range is well consistent with the heterophase state. We note that Rayleigh scattering vanishes in LNN12 where the rhombohedral *N* phase dominates unambiguously.

The concentration dependence of the full width at half maxima for both stretching modes is shown in Fig. 6. The width of each stretching mode steadily increases with increasing Li content due to disorder on the *A* sites in orthorhombic *P* and *Q* phases. At $x = 0.12$, both Nb-O stretching modes at 567 and 612 cm^{-1} exhibit very sharp narrowing. In the rhombohedral *N* phase both stretching bands are even

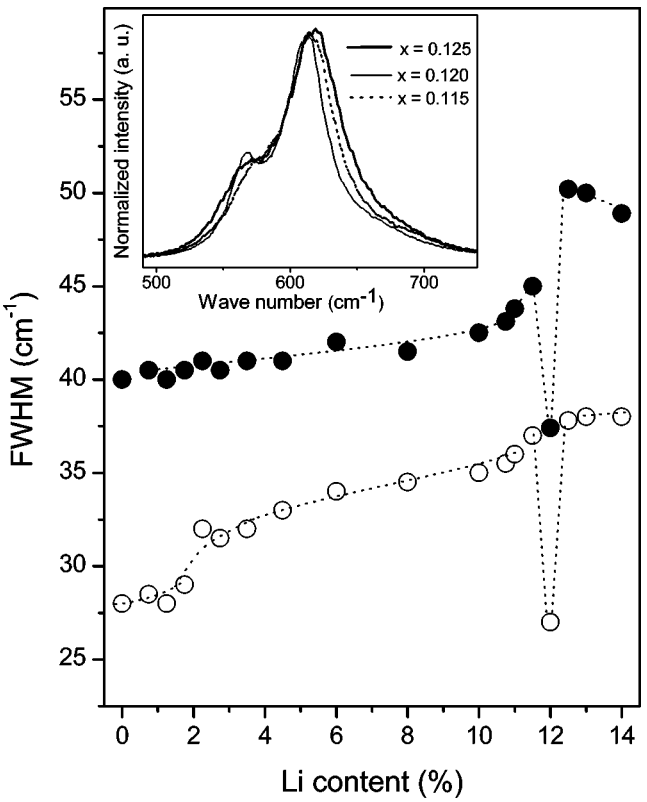

FIG. 6. Line width of Nb-O stretching vibrations (open symbols, 567 cm^{-1} peak; full symbols, 612 cm^{-1} peak) as a function of Li content. The inset shows the experimental spectra.

narrower than in pure $NaNbO_3$, which is a direct evidence of ordering in the crystal lattice. The high-frequency stretching mode is a simple breathing motion of the oxygen atoms and neither *A* nor *B* cations are involved into this vibration. However the *B* site cation can affect the frequency and the line shape through the *B*-O bond lengths. In the *N* phase the Nb ions are displaced from the central position, firmly localized, and have negligibly small amplitudes of thermal vibrations along the Nb-O bonds with the lengths 1.951 and 2.043 Å. In the *P* and *Q* phases there is a much broader distribution of the Nb-O bond lengths lying in the range from 1.857 to 2.110 Å (Ref. 15) and one expects larger widths of the stretching vibrations.

IV. SUMMARY AND CONCLUSIONS

The off-centering of the Nb ions within the NbO_6 group and the tilts of octahedra as rigid units are two crucial effects which give rise to numerous phase transitions in perovskites.[17] Of course, the Nb displacements and tilts of octahedra are not independent and influence one another. Our results show that substitution of Li for Na leads to serious changes in the crystal structure and increases the temperature of the phase transition into the *N* phase. Incorporation of Li ions with smaller size modifies electrostatic repulsion between Nb and *A* cation. At the same time changes in the polarization of the oxygen atoms surrounding the intervening sites disturb the delicate balance of the Nb-O bonds. In the concentration interval $0.02 \leqslant x \leqslant 0.03$ we have observed the *P*-*Q* transition where the change of *B* site displacement accompanied by rotations of octahedra occurred. Further increasing of Li content leads to disorder on the *A* sites, as revealed by the broadening of the Raman peaks.

The most interesting result is that the rhombohedral phase *N* of crystal structure very close to that obtained in pure $NaNbO_3$ below $-110\,^{\circ}C$ was disclosed for the sample with $x=0.12$ at room temperature. For this composition the tilt angle of octahedra about the triad axis increases very slightly and a distortion of the octahedra is observed in comparison with the low-temperature *N* phase of $NaNbO_3$. Evidently substitution of Li for Na induces displacements of the Nb ions along the triad axis and a triad-axis tilt of the NbO_6 octahedra only at particular concentration where $x \approx 1/8$. The value of $x=0.12$ corresponds approximately to one Li atom per doubled perovskite cell. One can assume that the majority of Li ions occupy *A* sites well disposed along the triad axis of the pseudocubic perovskite subcell and induce rhombohedral distortion at room temperature. Sharp reflections observed in XRD patterns and abrupt narrowing of Nb-O stretching peaks in the Raman spectrum suggest essentially high degree of order in the *N* phase dominating in the sample with $x=0.12$. However, this ordering is not complete because sufficiently large amount of the *Q* phase was also observed in this ceramic sample. An alteration of zones richer in one constituent than the other leads to coexistence of the *Q* and *N* phases in the concentration interval $0.10 \leqslant x \leqslant 0.14$ and only at $x=0.12$ the *N* phase unambiguously dominates.

Discrepancies between results reported by several groups concerning the range of stability of the rhombohedral phase in LNN solid solutions very probably originate due to differences in fabrication conditions and slight deviations from desirable stoichiometry. We have shown that FE rhombohedral phase can be stable at room temperature in LNN solid solutions, which makes this system attractive for applications in lead-free piezodevices.

ACKNOWLEDGMENTS

The authors gratefully thank L.A. Shilkina for enlightening discussions. This work was partially supported by the Russian Foundation for the Basic Research (Project No. 02-02-17781). Yuri Yuzyuk thanks Conseil Régional du Centre for Grant CE No.2001298011.

[1] N.N. Krainik, Izv. Akad. Nauk SSSR, Ser. Fiz. **22**, 1492 (1958); **28**, 643 (1964); Bull. Acad. Sci. USSR, Phys. Ser. (Engl. Transl.) **22**, 1486 (1958); **28**, 550 (1964).

[2] T. Nitta, J. Am. Ceram. Soc. **51**, 626 (1968).

[3] L.A. Reznitchenko and L.A. Shilkina, Izv. Akad. Nauk SSSR, Ser. Fiz. **39**, 1118 (1975); Bull. Acad. Sci. USSR, Phys. Ser. (Engl. Transl.) **39**, 187 (1975).

[4] L.A. Reznitchenko and L.A. Shilkina, Zh. Tekh. Fiz. **47**, 453

(1977) [Sov. Phys. Tech. Phys. **22**, 272 (1977)].
[5] L.A. Shilkina, L.A. Reznitchenko, M.F. Kupriyanov, and E.G. Fesenko, Zh. Tekh. Fiz. **47**, 2173 (1977) [Sov. Phys. Tech. Phys. **22**, 1262 (1977)].
[6] R. M Henson, R.R. Zeyfang, and K.V. Kiehl, J. Am. Ceram. Soc. **60**, 15 (1977).
[7] R. Von Der Mühll, A. Sadel, J. Ravez, and P. Hagenmuller, Solid State Commun. **31**, 151 (1979).
[8] Y.D. Juang, S.B. Dai, Y.C. Wang, W.Y. Chou, J.S. Hwang, M.L. Hu, and W.S. Tse, Solid State Commun. **111**, 723 (1999).
[9] Y.D. Juang, S.B. Dai, Y.C. Wang, J.S. Hwang, M.L. Hu, and W.S. Tse, J. Appl. Phys. **88**, 742 (2000).
[10] I. Pozdnyakova, A. Navrotsky, L. Shilkina, and L. Reznitchenko, J. Am. Ceram. Soc. **85**, 379 (2002).
[11] L.A. Reznitchenko, L.A. Shilkina, O.N. Razumovskaya, and S.I. Dudkina, Inorg. Mater. (Transl. Neorg. Mater.) **39**, 139 (2003).
[12] M. Gailhanou, J.M. Dubuisson, M. Ribbens, L. Roussier, D. Bétaille, C. Créoff, M. Lemonnier, J. Denoyer, C. Bouillot, A. Jucha, A. Lena, M. Idir, M. Bessière, D. Thiaudière, L. Hennet, C. Landron, and J.P. Coutures, Nucl. Instrum. Methods Phys. Res. A **467-468**, 745 (2001).
[13] H.D. Megaw and M. Wells, Acta Crystallogr. **11**, 858 (1958).
[14] M. Wells, H.D. Megaw, Proc. Phys. Soc. (London) **78**, 1258 (1961).
[15] A.C. Sakowski-Cowley, K. Lukaszewicz, and H.D. Megaw, Acta Crystallogr., Sect. B: Struct. Crystallogr. Cryst. Chem. **B25**, 851 (1969).
[16] E.S. Gagarina, L.A. Shilkina, L.A. Reznitchenko, I.P. Raevsky, V.G. Smotrakov, and V.V. Eremkin, Bull. Russ. Acad. Sci. Phys. **65**, 837 (2001).
[17] A.M. Glazer, Acta Crystallogr., Sect. A: Cryst. Phys., Diffr., Theor. Gen. Crystallogr. **31**, 756 (1975).
[18] C.N.W. Darlington and H.D. Megaw, Acta Crystallogr., Sect. B: Struct. Crystallogr. Cryst. Chem. **B29**, 2171 (1973).
[19] J. Rodriguez-Carvajal, Physica B **192**, 55 (1993); http://www-llb.cea.fr/fullweb/powder.htm
[20] V.A. Shuvaeva, M.Yu. Antipin, S.V. Lindeman, O.E. Fesenko, V.G. Smotrakov, and Yu.T. Struchkov, Ferroelectrics **141**, 307 (1993).
[21] H.D. Megaw, Acta Crystallogr., Sect. A: Cryst. Phys., Diffr., Theor. Gen. Crystallogr. **A24**, 583 (1968).
[22] http://www.chem.gla.ac.uk/~louis/software/ortep3
[23] E. Husson and Y. Repelin, Spectrochim. Acta, Part A **40**, 315 (1984).
[24] Z.X. Shen, X.B. Wang, M.H. Kuok, and S.H. Tang, J. Raman Spectrosc. **29**, 379 (1998).
[25] R.J.C. Lima, P.T.C. Freire, J.M.Sasaki.A.P. Ayala, F.E.A. Melo, J. Mendes Filho, K.C. Serra, S. Lanfredi, M.H. Lente, and J.A. Eiras, J. Raman Spectrosc. **33**, 669 (2002).
[26] E. Bouziane, M.D. Fontana, and M. Ayadi, J. Phys.: Condens. Matter **15**, 1387 (2003).